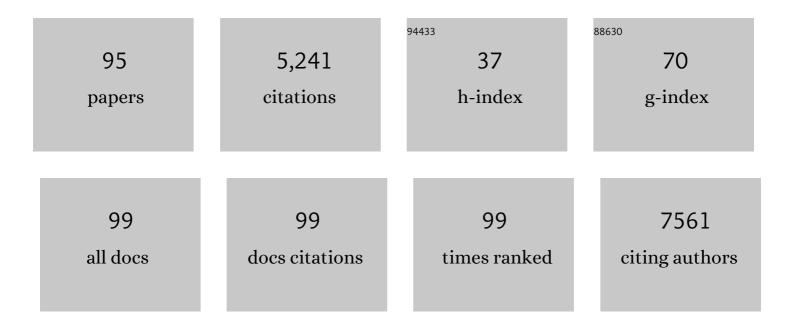
Mark A Isaacs

List of Publications by Year in descending order

Source: https://exaly.com/author-pdf/2555161/publications.pdf Version: 2024-02-01



#	Article	IF	CITATIONS
1	Continuous-flow synthesis of mesoporous SBA-15. Microporous and Mesoporous Materials, 2022, 329, 111535.	4.4	6
2	Integrated carbon capture and utilization: Synergistic catalysis between highly dispersed Ni clusters and ceria oxygen vacancies. Chemical Engineering Journal, 2022, 437, 135394.	12.7	33
3	Synthesis, characterisation, and feasibility studies on the use of vanadium tellurate(<scp>vi</scp>) as a cathode material for aqueous rechargeable Zn-ion batteries. RSC Advances, 2022, 12, 12211-12218.	3.6	2
4	Porous Dithiine-Linked Covalent Organic Framework as a Dynamic Platform for Covalent Polysulfide Anchoring in Lithium–Sulfur Battery Cathodes. Journal of the American Chemical Society, 2022, 144, 9101-9112.	13.7	71
5	P281 In vitro evaluation of the response of human tendon-derived stromal cells to a novel electrospun suture. Rheumatology, 2022, 61, .	1.9	0
6	Synergistic Effect of Simultaneous Doping of Ceria Nanorods with Cu and Cr on CO Oxidation and NO Reduction. Chemistry - A European Journal, 2021, 27, 2165-2174.	3.3	10
7	Mechanochemically synthesized Pb-free halide perovskite-based Cs ₂ AgBiBr ₆ –Cu–RGO nanocomposite for photocatalytic CO ₂ reduction. Journal of Materials Chemistry A, 2021, 9, 12179-12187.	10.3	70
8	Boosting the oxygen evolution activity in non-stoichiometric praseodymium ferrite-based perovskites by A site substitution for alkaline electrolyser anodes. Sustainable Energy and Fuels, 2021, 5, 154-165.	4.9	14
9	In vitro evaluation of the response of human tendonâ€derived stromal cells to a novel electrospun suture for tendon repair. Translational Sports Medicine, 2021, 4, 409-418.	1.1	6
10	Enhanced near-infrared absorption for laser powder bed fusion using reduced graphene oxide. Applied Materials Today, 2021, 23, 101009.	4.3	4
11	Degradation of Layered Oxide Cathode in a Sodium Battery: A Detailed Investigation by Xâ€Ray Tomography at the Nanoscale. Small Methods, 2021, 5, e2100596.	8.6	9
12	PdCu single atom alloys supported on alumina for the selective hydrogenation of furfural. Applied Catalysis B: Environmental, 2021, 299, 120652.	20.2	53
13	Advanced XPS characterization: XPS-based multi-technique analyses for comprehensive understanding of functional materials. Materials Chemistry Frontiers, 2021, 5, 7931-7963.	5.9	41
14	Palladium-doped hierarchical ZSM-5 for catalytic selective oxidation of allylic and benzylic alcohols. Royal Society Open Science, 2021, 8, 211086.	2.4	2
15	Band offsets of metal oxide contacts on TIBr radiation detectors. Journal of Applied Physics, 2021, 130, 175305.	2.5	0
16	Ru nanoparticles supported on N-doped reduced graphene oxide as valuable catalyst for the selective aerobic oxidation of benzyl alcohol. Catalysis Today, 2020, 357, 8-14.	4.4	30
17	Bandgap lowering in mixed alloys of Cs ₂ Ag(Sb _x Bi _{1â^'x})Br ₆ double perovskite thin films. Journal of Materials Chemistry A, 2020, 8, 21780-21788.	10.3	66
18	A spatially orthogonal hierarchically porous acid–base catalyst for cascade and antagonistic reactions. Nature Catalysis, 2020, 3, 921-931.	34.4	75

#	Article	IF	CITATIONS
19	Metal–Acid Synergy: Hydrodeoxygenation of Anisole over Pt/Alâ€&BAâ€15. ChemSusChem, 2020, 13, 4775-4	775.8	1
20	Ethanol Steam Reforming for Hydrogen Production Over Hierarchical Macroporous Mesoporous SBA-15 Supported Nickel Nanoparticles. Topics in Catalysis, 2020, 63, 403-412.	2.8	9
21	Shining light on the solid–liquid interface: <i>in situ</i> / <i>operando</i> monitoring of surface catalysis. Catalysis Science and Technology, 2020, 10, 5362-5385.	4.1	21
22	The origin of chemical inhomogeneity in garnet electrolytes and its impact on the electrochemical performance. Journal of Materials Chemistry A, 2020, 8, 14265-14276.	10.3	26
23	The effect of metal precursor on copper phase dispersion and nanoparticle formation for the catalytic transformations of furfural. Applied Catalysis B: Environmental, 2020, 273, 119062.	20.2	46
24	All-Inorganic CsPbBr ₃ Nanocrystals: Gram-Scale Mechanochemical Synthesis and Selective Photocatalytic CO ₂ Reduction to Methane. ACS Applied Energy Materials, 2020, 3, 4509-4522.	5.1	75
25	Carbon Nitride as a Ligand: Selective Hydrogenation of Terminal Alkenes Using [(Î- ⁵ ₅ Me ₅)IrCl(g ₃ N ₄ â€₽ ^{2Chemistry - A European Journal, 2020, 26, 6862-6868.}	> <iଃN\$,Nâ€</i	™ <u>∢/</u> ⊉>)]Cl.
26	Metal–Acid Synergy: Hydrodeoxygenation of Anisole over Pt/Al‧BAâ€15. ChemSusChem, 2020, 13, 4945-4953.	6.8	31
27	The antimicrobial efficacy of zinc doped phosphate-based glass for treating catheter associated urinary tract infections. Materials Science and Engineering C, 2019, 103, 109868.	7.3	16
28	Carbon nitride as a ligand: edge-site coordination of ReCl(CO) ₃ -fragments to g-C ₃ N ₄ . Chemical Communications, 2019, 55, 7450-7453.	4.1	10
29	Effect of Pt Promotion on the Ni-Catalyzed Deoxygenation of Tristearin to Fuel-Like Hydrocarbons. Catalysts, 2019, 9, 200.	3.5	16
30	Cascade Aerobic Selective Oxidation over Contiguous Dual-Catalyst Beds in Continuous Flow. ACS Catalysis, 2019, 9, 5345-5352.	11.2	20
31	Highly Selective and Solvent-Dependent Reduction of Nitrobenzene to <i>N</i> -Phenylhydroxylamine, Azoxybenzene, and Aniline Catalyzed by Phosphino-Modified Polymer Immobilized Ionic Liquid-Stabilized AuNPs. ACS Catalysis, 2019, 9, 4777-4791.	11.2	77
32	Unravelling mass transport in hierarchically porous catalysts. Journal of Materials Chemistry A, 2019, 7, 11814-11825.	10.3	57
33	Atomically dispersed nickel as coke-resistant active sites for methane dry reforming. Nature Communications, 2019, 10, 5181.	12.8	398
34	Mesoporous NiO/Al-SBA-15 catalysts for solvent-free deoxygenation of palm fatty acid distillate. Microporous and Mesoporous Materials, 2019, 276, 13-22.	4.4	68
35	Development of Ca/KIT-6 adsorbents for high temperature CO2 capture. Fuel, 2019, 235, 1070-1076.	6.4	31
36	The Antimicrobial Efficacy of Hypoxia Mimicking Cobalt Oxide Doped Phosphate-Based Glasses against Clinically Relevant Gram Positive, Gram Negative Bacteria and a Fungal Strain. ACS Biomaterials Science and Engineering, 2019, 5, 283-293.	5.2	16

#	Article	IF	CITATIONS
37	Platinum catalysed aerobic selective oxidation of cinnamaldehyde to cinnamic acid. Catalysis Today, 2019, 333, 161-168.	4.4	18
38	Insight into the atomic scale structure of CaF2-CaO-SiO2 glasses using a combination of neutron diffraction, 29Si solid state NMR, high energy X-ray diffraction, FTIR, and XPS. Biomedical Glasses, 2019, 5, 112-123.	2.4	4
39	MoS2 and WS2 nanocone arrays: Impact of surface topography on the hydrogen evolution electrocatalytic activity and mass transport. Applied Materials Today, 2018, 11, 70-81.	4.3	33
40	Synthesis of Amine Functionalized Mesoporous Silicas Templated by Castor Oil for Transesterification. MRS Advances, 2018, 3, 2261-2269.	0.9	6
41	Zirconia catalysed acetic acid ketonisation for pre-treatment of biomass fast pyrolysis vapours. Catalysis Science and Technology, 2018, 8, 1134-1141.	4.1	31
42	Solution-processable, niobium-doped titanium oxide nanorods for application in low-voltage, large-area electronic devices. Journal of Materials Chemistry C, 2018, 6, 1038-1047.	5.5	5
43	Hydrogen evolution enhancement of ultra-low loading, size-selected molybdenum sulfide nanoclusters by sulfur enrichment. Applied Catalysis B: Environmental, 2018, 235, 84-91.	20.2	56
44	Single atom Cu(I) promoted mesoporous titanias for photocatalytic Methyl Orange depollution and H2 production. Applied Catalysis B: Environmental, 2018, 232, 501-511.	20.2	75
45	Magnetically-separable Fe3O4@SiO2@SO4-ZrO2 core-shell nanoparticle catalysts for propanoic acid esterification. Molecular Catalysis, 2018, 449, 137-141.	2.0	15
46	Delaminated CoAl‣ayered Double Hydroxide@TiO ₂ Heterojunction Nanocomposites for Photocatalytic Reduction of CO ₂ . Particle and Particle Systems Characterization, 2018, 35, 1700317.	2.3	40
47	Citrate-mediated sol–gel synthesis of Al-substituted sulfated zirconia catalysts for α-pinene isomerization. Molecular Catalysis, 2018, 458, 206-212.	2.0	11
48	Alkali-Free Zn–Al Layered Double Hydroxide Catalysts for Triglyceride Transesterification. Catalysts, 2018, 8, 667.	3.5	9
49	Sulfated Zirconia Catalysts for D-Sorbitol Cascade Cyclodehydration to Isosorbide: Impact of Zirconia Phase. ACS Sustainable Chemistry and Engineering, 2018, 6, 14704-14712.	6.7	25
50	Gold-catalyzed conversion of lignin to low molecular weight aromatics. Chemical Science, 2018, 9, 8127-8133.	7.4	61
51	Tunable Silver-Functionalized Porous Frameworks for Antibacterial Applications. Antibiotics, 2018, 7, 55.	3.7	7
52	On the Impact of the Preparation Method on the Surface Basicity of Mg–Zr Mixed Oxide Catalysts for Tributyrin Transesterification. Catalysts, 2018, 8, 228.	3.5	10
53	Optimization of ruthenium based catalysts for the aqueous phase hydrogenation of furfural to furfuryl alcohol. Applied Catalysis A: General, 2018, 563, 177-184.	4.3	45
54	A porous activated carbon supported Pt catalyst for the oxidative degradation of poly[(naphthaleneformaldehyde)sulfonate]. Journal of the Taiwan Institute of Chemical Engineers, 2018, 93, 289-297.	5.3	7

#	Article	IF	CITATIONS
55	Sizeâ€Dependent Visible Light Photocatalytic Performance of Cu ₂ O Nanocubes. ChemCatChem, 2018, 10, 3554-3563.	3.7	44
56	Support enhanced α-pinene isomerization over HPW/SBA-15. Applied Catalysis B: Environmental, 2017, 200, 10-18.	20.2	72
57	On the Mn promoted synthesis of higher alcohols over Cu derived ternary catalysts. Catalysis Science and Technology, 2017, 7, 988-999.	4.1	31
58	High activity magnetic core-mesoporous shell sulfonic acid silica nanoparticles for carboxylic acid esterification. Catalysis Communications, 2017, 92, 56-60.	3.3	29
59	Paternal low protein diet programs preimplantation embryo gene expression, fetal growth and skeletal development in mice. Biochimica Et Biophysica Acta - Molecular Basis of Disease, 2017, 1863, 1371-1381.	3.8	51
60	On the influence of Si:Al ratio and hierarchical porosity of FAU zeolites in solid acid catalysed esterification pretreatment of bio-oil. Biomass Conversion and Biorefinery, 2017, 7, 331-342.	4.6	50
61	Regioselective Baeyer–Villiger oxidation of lignin model compounds with tin beta zeolite catalyst and hydrogen peroxide. RSC Advances, 2017, 7, 25987-25997.	3.6	35
62	Tunable Ag@SiO ₂ core–shell nanocomposites for broad spectrum antibacterial applications. RSC Advances, 2017, 7, 23342-23347.	3.6	10
63	Bio-oil upgrading via vapor-phase ketonization over nanostructured FeOx and MnOx: catalytic performance and mechanistic insight. Biomass Conversion and Biorefinery, 2017, 7, 319-329.	4.6	14
64	P25@CoAl layered double hydroxide heterojunction nanocomposites for CO 2 photocatalytic reduction. Applied Catalysis B: Environmental, 2017, 209, 394-404.	20.2	200
65	NiO/nanoporous carbon heterogeneous Fenton catalyst for aqueous microcystine-LR decomposition. Journal of the Taiwan Institute of Chemical Engineers, 2017, 74, 289-295.	5.3	11
66	A new application for transition metal chalcogenides: WS2 catalysed esterification of carboxylic acids. Catalysis Communications, 2017, 91, 16-20.	3.3	17
67	Tailored mesoporous silica supports for Ni catalysed hydrogen production from ethanol steam reforming. Catalysis Communications, 2017, 91, 76-79.	3.3	51
68	Development and Characterization of Gallium-Doped Bioactive Glasses for Potential Bone Cancer Applications. ACS Biomaterials Science and Engineering, 2017, 3, 3425-3432.	5.2	31
69	Dual Wavelength (Ultraviolet and Green) Photodetectors Using Solution Processed Zinc Oxide Nanoparticles. ACS Applied Materials & amp; Interfaces, 2017, 9, 36971-36979.	8.0	13
70	Classical strong metal–support interactions between gold nanoparticles and titanium dioxide. Science Advances, 2017, 3, e1700231.	10.3	361
71	H5PW10V2O40@VOx/SBA-15-NH2 catalyst for the solventless synthesis of 3-substituted indoles. Tetrahedron, 2017, 73, 5862-5871.	1.9	23
72	Active Site Elucidation and Optimization in Pt Co atalysts for Photocatalytic Hydrogen Production over Titania. ChemCatChem, 2017, 9, 4268-4274.	3.7	21

#	Article	IF	CITATIONS
73	A magnetically-separable H 3 PW 12 O 40 @Fe 3 O 4 /EN-MIL-101 catalyst for the one-pot solventless synthesis of 2H-indazolo[2,1- b] phthalazine-triones. Molecular Catalysis, 2017, 440, 96-106.	2.0	42
74	Multi-Dimensional Multi-Functional Catalytic Architecture: A Selectively Functionalized Three-Dimensional Hierarchically Ordered Macro/Mesoporous Network for Cascade Reactions Analyzed by Electron Tomography. Microscopy and Microanalysis, 2017, 23, 2042-2043.	0.4	3
75	Electrochemical sulfidation of WS 2 nanoarrays: Strong dependence of hydrogen evolution activity on transition metal sulfide surface composition. Electrochemistry Communications, 2017, 81, 106-111.	4.7	18
76	Impact of Macroporosity on Catalytic Upgrading of Fast Pyrolysis Bioâ€Oil by Esterification over Silica Sulfonic Acids. ChemSusChem, 2017, 10, 3506-3511.	6.8	24
77	Acetic Acid Ketonization over Fe ₃ O ₄ /SiO ₂ for Pyrolysis Bioâ€Oil Upgrading. ChemCatChem, 2017, 9, 1648-1654.	3.7	47
78	Cobalt promoted TiO2/GO for the photocatalytic degradation of oxytetracycline and Congo Red. Applied Catalysis B: Environmental, 2017, 201, 159-168.	20.2	298
79	Acidity-Reactivity Relationships in Catalytic Esterification over Ammonium Sulfate-Derived Sulfated Zirconia. Catalysts, 2017, 7, 204.	3.5	41
80	Cu and Fe oxides dispersed on SBA-15: A Fenton type bimetallic catalyst for N,N -diethyl- p -phenyl diamine degradation. Applied Catalysis B: Environmental, 2016, 199, 323-330.	20.2	119
81	Pore confinement effects and stabilization of carbon nitride oligomers in macroporous silica for photocatalytic hydrogen production. Carbon, 2016, 106, 320-329.	10.3	19
82	Platinum-Catalyzed Aqueous-Phase Hydrogenation of <scp>d</scp> -Glucose to <scp>d</scp> -Sorbitol. ACS Catalysis, 2016, 6, 7409-7417.	11.2	94
83	Niobic acid nanoparticle catalysts for the aqueous phase transformation of glucose and fructose to 5-hydroxymethylfurfural. Catalysis Science and Technology, 2016, 6, 7334-7341.	4.1	29
84	Spatially orthogonal chemical functionalization ofÂa hierarchical pore network for catalytic cascadeÂreactions. Nature Materials, 2016, 15, 178-182.	27.5	101
85	Photodeposition as a facile route to tunable Pt photocatalysts for hydrogen production: on the role of methanol. Catalysis Science and Technology, 2016, 6, 81-88.	4.1	65
86	Electrocatalytic regeneration of atmospherically aged MoS ₂ nanostructures via solution-phase sulfidation. RSC Advances, 2016, 6, 26689-26695.	3.6	5
87	Bio-inspired carbon electro-catalysts for the oxygen reduction reaction. Journal of Energy Chemistry, 2016, 25, 228-235.	12.9	25
88	Facile synthesis of hierarchical Cu2O nanocubes as visible light photocatalysts. Applied Catalysis B: Environmental, 2016, 189, 226-232.	20.2	132
89	Effect of Cu and Sn promotion on the catalytic deoxygenation of model and algal lipids to fuel-like hydrocarbons over supported Ni catalysts. Applied Catalysis B: Environmental, 2016, 191, 147-156.	20.2	102
90	The surface chemistry of nanocrystalline MgO catalysts for FAME production: An in situ XPS study of H2O, CH3OH and CH3OAc adsorption. Surface Science, 2016, 646, 170-178.	1.9	40

#	Article	IF	CITATIONS
91	Highly selective hydrogenation of furfural over supported Pt nanoparticles under mild conditions. Applied Catalysis B: Environmental, 2016, 180, 580-585.	20.2	288
92	Solid base catalysed 5-HMF oxidation to 2,5-FDCA over Au/hydrotalcites: fact or fiction?. Chemical Science, 2015, 6, 4940-4945.	7.4	125
93	Facile route to conformal hydrotalcite coatings over complex architectures: a hierarchically ordered nanoporous base catalyst for FAME production. Green Chemistry, 2015, 17, 2398-2405.	9.0	30
94	Selectivity control in Pt-catalyzed cinnamaldehyde hydrogenation. Scientific Reports, 2015, 5, 9425.	3.3	101
95	Ag Alloyed Pd Single-Atom Catalysts for Efficient Selective Hydrogenation of Acetylene to Ethylene in Excess Ethylene. ACS Catalysis, 2015, 5, 3717-3725.	11.2	545